Eur J Nucl Med Mol Imaging (2010) 37:1148–1155
DOI 10.1007/s00259-010-1405-5

ORIGINAL ARTICLE

Anatomy-based reconstruction of FDG-PET images with implicit partial volume correction improves detection of hypometabolic regions in patients with epilepsy due to focal cortical dysplasia diagnosed on MRI

Karolien Goffin · Wim Van Paesschen · Patrick Dupont · Kristof Baete · André Palmini · Johan Nuyts · Koen Van Laere

Received: 17 September 2009 / Accepted: 3 February 2010 / Published online: 20 March 2010

Abstract
Purpose Detection of hypometabolic areas on interictal FDG-PET images for assessing the epileptogenic zone is hampered by partial volume effects. We evaluated the performance of an anatomy-based maximum a-posteriori (A-MAP) reconstruction algorithm which combined noise suppression with correction for the partial volume effect in the detection of hypometabolic areas in patients with focal cortical dysplasia (FCD).
Methods FDG-PET images from 14 patients with refractory partial epilepsy were reconstructed using A-MAP and maximum likelihood (ML) reconstruction. In all patients, presurgical evaluation showed that FCD represented the epileptic lesion. Correspondence between the FCD location and regional metabolism on a predefined atlas was evaluated. An asymmetry index of FCD to normal cortex was calculated.
Results Hypometabolism at the FCD location was detected in 9/14 patients (64%) using ML and in 10/14 patients (71%) using A-MAP reconstruction. Hypometabolic areas outside the FCD location were detected in 12/14 patients (86%) using ML and in 11/14 patients (79%) using A-MAP reconstruction. The asymmetry index was higher using A-MAP reconstruction (0.61, ML 0.49, p=0.03).
Conclusion The A-MAP reconstruction algorithm improved visual detection of epileptic FCD on brain FDG-PET images compared to ML reconstruction, due to higher contrast and better delineation of the lesion. This improvement failed to reach significance in our small sample. Hypometabolism outside the lesion is often present, consistent with the observation that the functional deficit zone tends to be larger than the epileptogenic zone.

Keywords FDG-PET · A-MAP · FCD · Hypometabolism

K. Goffin (✉) · P. Dupont · K. Baete · J. Nuyts · K. Van Laere
Division of Nuclear Medicine and Medical Imaging Center,
University Hospital Leuven,
Herestraat 49,
3000 Leuven, Belgium
e-mail: Karolien.Goffin@uzleuven.be

W. Van Paesschen
Neurology Department, University Hospital Leuven,
Herestraat 49,
3000 Leuven, Belgium

P. Dupont
Laboratory of Cognitive Neurology, University Hospital Leuven,
Herestraat 49,
3000 Leuven, Belgium

A. Palmini
Porto Alegre Epilepsy Surgery Program, Hospital São Lucas,
Pontificia Universidade Catolica do Rio Grande do Sul (PUCRS),
Avenida Ipiranga 6690,
90610-000 Porto Alegre, Brazil

Introduction

Epileptic seizures are the result of abnormal discharges of a group of nerve cells in specific areas in the grey matter (GM) tissue of the brain [1]. Malformations caused by abnormalities of cortical development (MCD) are a common cause of intractable focal epilepsy [2]. Focal cortical dysplasia (FCD), characterized by abnormal neuroglial proliferation, is the most frequent MCD in patients referred for presurgical evaluation [3, 4]. The histopathology of FCDs is classified into mild Palmini type I and severe

Palmini type II [5]. Type I FCDs are characterized by architectural abnormalities (dyslamination and other mild abnormalities) with (Ib) or without (Ia) 'immature' or giant neurons. In type II FCDs, dysmorphic neurons with (IIb) or without (IIa) balloon cells are also present [5].

Surgical resection of the FCD renders 33–75% of individuals seizure-free [6]. The key to the success of resective surgery is the accurate localization of the region of seizure onset. On magnetic resonance imaging (MRI), variable degrees of cortical thickening, blurring of the cortex/white matter junction, hyperintense signal on T2-weighted, proton density, or fluid-attenuated inversion recovery (FLAIR) sequences, and extension of cortical tissue with increased signal from the surface to the ventricle may be present in patients with FCD [5]. These lesions, however, are often very subtle and difficult to detect on standard MR images.

Interictal positron emission tomography (PET) of glucose metabolism, using 2-[^{18}F]fluoro-2-deoxy-D-glucose (FDG) has been shown to be a useful and sensitive imaging method for delineating lesions of focal cortical dysgenesis in infants [7–11]. In a study of adults with surgically proven FCD, interictal cortical hypometabolism at the focus of the lesion on FDG-PET was present in 85–90% of the patients [12]. According to Otsuki, interictal FDG-PET may be more sensitive in the detection of FCD than MRI, interictal single photon emission computed tomography (SPECT) and magnetoencephalography [13]. In patients with neocortical epilepsy, hypometabolism on FDG-PET images is a significant positive prognostic factor for a postsurgical seizure-free outcome, next to the presence of a focal lesion on MRI and localized ictal rhythms on electroencephalography (EEG) [14].

The hypometabolic areas on FDG-PET images corresponding to the FCD can however be very subtle and difficult to detect. The main reasons for this detection problem are the limited spatial resolution of the PET system and the noise affecting PET images [15]. The average GM thickness, which is about 3 mm [16], is relatively small compared to the spatial resolution of the current mainstream PET systems, which is about 5 mm, and to the voxel size used for brain PET imaging, which is typically about 2 mm in all directions. Since the thickness and geometry of the GM varies in the human brain, measuring small brain structures will lead to an underestimation of tracer activity. This well-known partial volume effect (PVE) can lead to spurious hypometabolic regions, resulting in an increased amount of false-positive hypometabolic regions. Moreover, because of the finite spatial resolution of the imaging system, a spillover of activity to neighbouring regions can occur, leading to a misinterpretation of the extent of hypometabolic regions.

The anatomy-based maximum a-posteriori iterative reconstruction algorithm (A-MAP) has recently been developed to correct for this PVE, and improves the detection of subtle regions of hypometabolism on FDG-PET images [17]. The A-MAP algorithm includes the anatomical information of a brain MR image as a priori knowledge in a Bayesian reconstruction framework. When this information is used together with a model for the finite system resolution, it yields strong PVE correction near boundaries between different tissue classes, in particular for structures with small dimensions such as the GM. It has been shown that the use of the A-MAP algorithm improves the detection accuracy of small hypometabolic regions on two-dimensional (2-D) simulated FDG-PET images of the brain in a human observer study, compared to post-smoothed maximum-likelihood reconstruction (ML) [18]. In the A-MAP approach, the PVE correction is done during reconstruction. Alternatively, partial volume correction can be implemented as a postprocessing technique, to be applied to an unconstrained ML reconstruction with resolution recovery. However, a comparison of the two approaches with theoretical analysis and with simulations [19] revealed more adverse noise propagation for the postcorrection method.

In this study, we investigated the detection accuracy of FDG-PET in patients with an MRI-defined FCD as epileptic lesion and evaluated the usefulness of the A-MAP reconstruction algorithm compared to standard postsmoothed ML reconstruction.

Materials and methods

Patient characteristics

A total of 14 patients with refractory partial epilepsy (seven men, seven women; mean age 38±11 years) who had undergone a brain PET investigation with ^{18}F-FDG between September 2000 and July 2004 as part of their presurgical diagnostic programme were studied retrospectively. The mean disease duration was 25±13 years at the time of PET scanning.

The epileptogenic zone was defined using a combination of seizure semiology, interictal and ictal EEG, optimized MRI, ictal and interictal ^{99m}Tc-ECD brain perfusion SPECT imaging and SISCOM (subtraction ictal SPECT coregistered to MRI) analysis. In all patients, a lesion with the MR characteristics of a FCD was the epileptic lesion. Six lesions were located in the temporal lobe, five in the frontal lobe, two in the parietal lobe and one in the insula. Eight patients underwent epilepsy surgery. Five patients were rendered seizure-free (Engel I), one almost seizure-free (Engel II) and two had a worthwhile improvement (Engel III) [20]. Resection specimens showed cortical dysplasia type I (n=1), type IIA (n=3), type IIB (n=1), gliosis (n=1), spongiosis (n=1) and no abnormalities (n=1). The mean

postoperative follow-up period was 3.4±2.1 years. The patient characteristics are given in Table 1. The lesion was unresectable in the other six patients because of its location near or in the eloquent cortex.

Fifteen healthy age-matched controls were available from a previous study [21].

Imaging

PET scans were obtained in the interictal state with ^{18}F-FDG under standard resting conditions (eyes closed in dimmed ambient light) using an ECAT EXACT HR+ PET scanner (Siemens, Knoxville, TN). A transmission scan of 10 min using ^{68}Ge rod sources was acquired in 2-D mode to correct for photon attenuation. A 3-D mode emission scan of 30 minutes was started 30 min after intravenous injection of 150 MBq ^{18}F-FDG. Continuous EEG monitoring was performed before injection and during the uptake period of ^{18}F-FDG into the brain to confirm the interictal state.

All subjects underwent high-resolution MR imaging with a T1-weighted magnetization prepared rapid acquisition gradient echo sequence (3D-MPRAGE; voxel-size 0.98×0.98×1.20 mm^3), a T2-weighted sequence and a FLAIR sequence. MR imaging was performed on a 1.5 T Vision Scanner (Siemens, Erlangen, Germany).

Image processing

FDG-PET data were reconstructed using the ML algorithm with resolution recovery and A-MAP algorithm as described previously [17, 18]. The transmission scan was reconstructed using a maximum a-posteriori reconstruction algorithm. Randoms correction of the 3-D emission scan was performed on-line using a delayed time window. The reconstructed attenuation image was used to apply correction for attenuation and scatter to the 3-D emission data, followed by the Fourier rebinning algorithm. The obtained 2-D projection data were reconstructed using ML. To approximately restore the Poisson statistics, the 2D data were uncorrected for attenuation prior to reconstruction. We included correction for the attenuation and for finite spatial resolution in the ML reconstruction. The resolution recovery assumed a shift-invariant gaussian blurring with a full-width at half-maximum (FWHM) of 5 mm.

Segmentation of the GM, white matter and cerebrospinal fluid tissues was performed using the Statistical Parametric Mapping (SPM2) software package (Wellcome Trust Centre for Neuroimaging, London, UK; http://www.fil.ion.ucl.ac.uk/spm). The rigid transformation was computed to align the MR image with the postsmoothed ML reconstruction of the PET data. Then, the same transformation was used to align the segmentation images of the MRI data with the ML reconstruction. The anatomical information was resampled to the PET grid (voxel size 2.25×2.25×2.43 mm^3) using linear interpolation. The ML reconstruction, postsmoothed using a gaussian kernel with 5 mm FWHM, was used as the initial image for the A-MAP iterative reconstruction. We used the same iteration scheme, attenuation correction and resolution recovery as for the ML reconstruction. For further image processing and analysis, ML reconstructed images were spatially normalized to the PET-template available in SPM2 using nonlinear warping (7×9×7 basis functions, 16 iterations) and the transformation was applied to the A-MAP reconstructed images.

Evaluation

Visual analysis

For visual analysis of FDG-PET data, a set of volumes-of-interest (VOIs) created in-house was used, which were defined according to Brodmann areas with the aid of the Talairach atlas [22], using PMOD v2.65 (PMOD, Zurich, Switzerland), as described previously (37 Brodmann areas per hemisphere) [23]. To adjust to the image characteristics of normal ML and A-MAP reconstructed images, scans of 15 healthy controls, reconstructed with the same dual parameter settings, were analyzed. Afterwards, both sets of FDG-PET images of patients were visually evaluated by two experienced nuclear medicine physicians blinded to the results of other investigations and to patient data, including MRI, to identify cortical VOIs with decreased metabolism. The final locations of hypometabolism were reached by consensus. Correspondences between VOIs containing the lesion and hypometabolic cortical VOIs, as detected blindly on FDG-PET images, were evaluated for both ML and A-MAP reconstructed images. Hypometabolism at the lesion was also compared between the two reconstruction techniques on a patient basis. Using the coregistered MR images, hypometabolism at the location of the FCD on MR images was assessed visually on ML and A-MAP reconstructed images.

For statistical comparisons, the McNemar test was used to compare ML and A-MAP reconstructions (Statistica, version 7; Statsoft, Tulsa, OK). P values <0.05 were considered statistically significant.

Asymmetry index

On MR images, the FCD was delineated manually and the VOI was mirrored and transferred to the contralateral normal cortex (Fig. 1). Average and minimal uptake values within the VOIs were calculated on ML and A-MAP reconstructed images using PMOD v2.65 (PMOD, Zurich, Switzerland). An asymmetry index of the FCD compared to the normal contralateral cortex was calculated as 1 − (minimal uptake value in FCD/average uptake value in the contralateral

Table 1 Patient characteristics

Patient no.	Sex	Age (years)	Age at onset (years)	Disease duration (years)	Location of FCD	Surgery	Histopathology	Surgical outcome	ML-positive	A-MAP-positive	Extralesional hypometabolism	
											ML	A-MAP
1	M	17	12	5	Right temporal (BA 20, 21, 28, 36, 38)	Incomplete lesion resection	CD IIA	Engel III	Yes	Yes	Superior and occipitotemporal	Superior and occipitotemporal
2	M	29	3	26	Left parietal (BA 22, 40, 41, 42, 48)	–	–	–	Yes	Yes	Infero-, mid-, occipitotemporal; cuneus; midfrontal	Infero-, mid-, occipitotemporal; cuneus
3	F	49	6	43	Left parietal (BA 39)	–	–	–	Yes	Yes	Occipitotemporal	–
4	F	40	33	7	Left temporal (BA 20, 28, 34, 35, 36, 38)	Lesion resection	CD I	Engel III	Yes	Yes	Mid-, superior temporal; midfrontal	Mid-, superior temporal; midfrontal
5	M	35	12	23	Right parietal (BA 40)	Lesion resection	CD IIB	Engel I	Yes	Yes	Orbitofrontal; gyrus postcentralis	Entorhinal; infero-, midfrontal
6	M	51	20	31	Right temporal (BA 20, 21, 28, 34, 35, 36, 37)	–	–	–	Yes	Yes	Superior temporal; temporopolar; infero-, midfrontal; cuneus; insula	Superior temporal; temporopolar; infero-, midfrontal
7	F	22	6	16	Left temporal (BA 21, 22, 37, 40)	–	–	–	Yes	Yes	Inferotemporal; temporopolar; cuneus	Inferotemporal; temporopolar; cuneus
8	F	53	12	41	Left frontal (BA 6–9)	–	–	–	No	Yes	–	–
9	M	48	16	32	Left frontal (BA 44, 46)	Lesion resection (2003 and 2006)	Gliosis	Engel I	Yes	Yes	–	–
10	M	31	23	8	Left frontal (BA 24)	Lesion resection (2004 and 2006)	CD IIA	Engel I	No	No	Infero-, midtemporal; temporopolar; entorhinal; superior parietal	Infero-, midtemporal; temporopolar
11	F	46	6	40	Left frontocentral (BA 20, 35, 36, 37)	Lesion resection	No abnormalities	Engel II	No	No	Posterior temporal	Gyrus angularis; posterior temporal
12	M	27	6	21	Right temporal (BA 47, 48)	Lesion resection	CD IIA	Engel I	Yes	Yes	Infero-, mid-, superior temporal; temporopolar; gyrus angularis; cuneus	Infero-, mid-, superior temporal; temporopolar; gyrus angularis; cuneus
13	F	34	10	24	Left insular cortex (BA 6)	–	–	–	No	No	Superior frontal; anterior cingulate	Superior frontal; anterior cingulate
14	F	45	11	34	Left frontal (BA 8, 9)	Lesion resection	Spongiosis	Engel I	No	No	Infero-, mid-, superior, occipitotemporal; temporopolar; orbitofrontal; cuneus	Infero-, mid-, superior, occipitotemporal; temporopolar; orbitofrontal; cuneus

BA Brodmann area

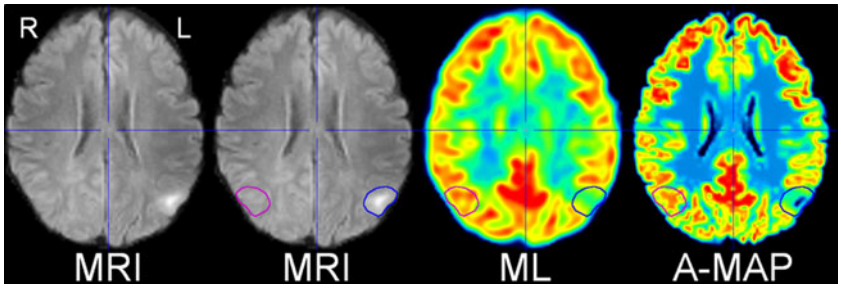

Fig. 1 FLAIR, ML and A-MAP reconstructed FDG-PET images from a patient with FCD in the left posterior parietal cortex (patient 3) (*blue VOI*) and mirrored VOI on the normal contralateral cortex (*purple VOI*). Images are coregistered

cortex). The asymmetry index was compared between ML and A-MAP reconstructed images using the paired Student's *t*-test. Data are reported as means±SD.

Results

We detected a mean of 8.2±5.2 hypometabolic cortical VOIs per patient (range 1–14) on ML reconstructed images and 7.3±4.5 (range 1–14) on A-MAP reconstructed images. On MR images, lesions corresponded to 3.1±2.1 VOIs (range 1–7; Table 1), depending on lesion size. Hypometabolism was present in 25/43 lesion VOIs (58%) using ML reconstruction and in 29/43 (67%) using A-MAP reconstruction (p=0.29). On ML and A-MAP reconstructed images, 72/115 (63%) and 59/102 (58%) hypometabolic cortical areas, respectively, were located outside the lesion. These extralesional hypometabolic areas were most often located around the lesion. In four patients, supplementary hypometabolism in the mid- and orbitofrontal areas was noted (Table 1). This corresponded to 5.1±3.8 hypometabolic cortical areas outside the lesion per patient on ML reconstructed images (range 0–10) and 4.2±3.2 on A-MAP reconstructed images (range 0–10).

On a patient basis, hypometabolism at the lesion was detected in 10/14 patients (71%) using A-MAP reconstruction, and in 9/14 patients (64%) using ML reconstruction (p>0.05). In one patient, hypometabolism at the FCD located in the left superior frontal cortex was only detected on A-MAP reconstructed FDG-PET images, and not on ML reconstructed images (Fig. 2). Reviewer 1 detected hypometabolism at the lesion in 9/14 patients using both A-MAP and ML reconstruction. The detection rate of reviewer 2 improved from 4/14 patients using ML reconstruction to 6/14 patients using A-MAP reconstruction. Hypometabolic cortical areas outside the FCD location were detected in 12/14 patients (86%) and in 11/14 patients (79%) using ML and A-MAP reconstruction, respectively (p>0.05).

The asymmetry index of the lesional to normal cortex was significantly higher in A-MAP reconstructed images

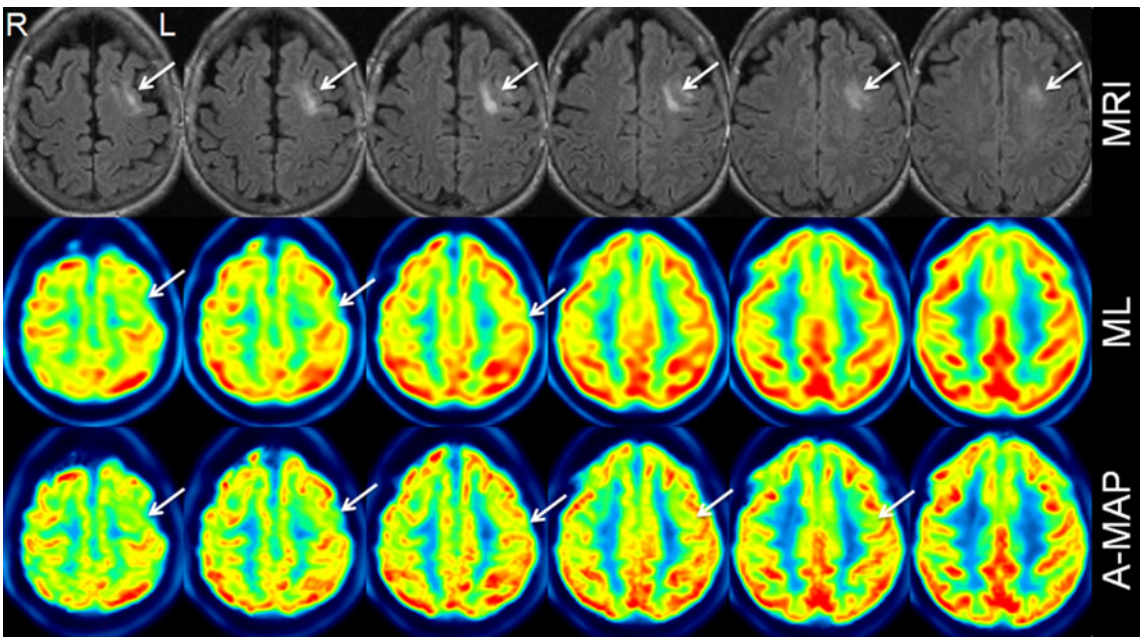

Fig. 2 FLAIR, ML and A-MAP reconstructed FDG-PET images from a patient with FCD in the left superior frontal cortex (patient 8). Blinded visual interpretation of ML FDG-PET images was negative. A hypometabolic area was, however, detected on A-MAP reconstructed FDG-PET images at the location of the FCD. Images are coregistered

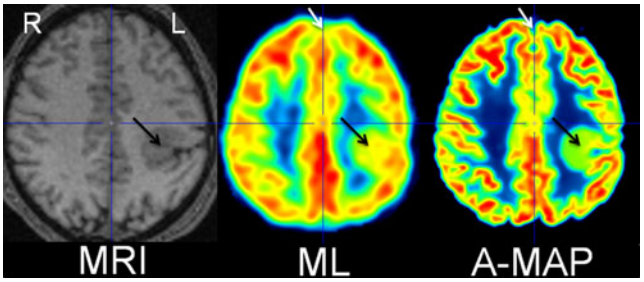

Fig. 3 T1, ML and A-MAP reconstructed FDG-PET images from a patient with FCD in the left parietal cortex (patient 2) (*black arrows*). ML FDG-PET images show hypometabolism in the medial frontal cortex bilaterally (*white arrow*). This hypometabolism is not seen on A-MAP reconstructed FDG-PET images (*white arrow*), suggesting its false-positive character. Images are coregistered

than in ML reconstructed images (0.61±0.18 vs. 0.49±0.13; p=0.03).

When using FDG-PET/MRI coregistration for assessing hypometabolism at the FCD-VOI visually, the detection rate of hypometabolism increased to 11/14 patients (79%) in ML reconstructed images and to 12/14 (86%) in A-MAP reconstructed images (p>0.05).

Discussion

Detection of hypometabolic areas on FDG-PET images can be difficult due to PVEs, but is important when assessing the epileptogenic zone in patients with FCD. Over the last decade, many groups have developed techniques to correct for PVE using anatomical information from segmented MR images after the reconstruction process or as a priori knowledge in the reconstruction framework [18, 24, 25]. Although PVE-corrected FDG-PET images are likely to be superior in diagnosing neurodegenerative disorders [26], no studies have been performed so far to evaluate the superiority of these reconstruction techniques for FDG-PET images in epilepsy. In patients with temporal lobe epilepsy caused by hippocampal sclerosis, who have focal gliosis and neuronal loss in the hippocampus, amygdala and entorhinal cortex, the importance of the use of partial volume correction has been demonstrated for PET measurements of cerebral metabolic rate for glucose [27], cerebral blood flow [28], and serotonergic 5-HT_{1A} [29] and central benzodiazepine receptors [30, 31]. We evaluated the performance of the A-MAP reconstruction algorithm, which inherently applies partial volume correction for activity in the GM region, in the detection of hypometabolic areas on FDG-PET images in a group of patients with FCD. We had already shown that the A-MAP reconstruction technique improves the detection rate of small hypometabolic areas in a human observer study using 2-D simulated FDG-PET images of the brain compared to ML reconstruction [18].

In the present study, we showed that the A-MAP reconstruction technique improved the visual blinded detection of hypometabolic cortical areas on FDG-PET images associated with epileptic FCD, on a lesion VOI basis as well as on a patient basis. This improvement failed to reach significance in our small sample. Overall, the epileptogenic foci were detected in 71% and 64% of patients on A-MAP reconstruction and ML

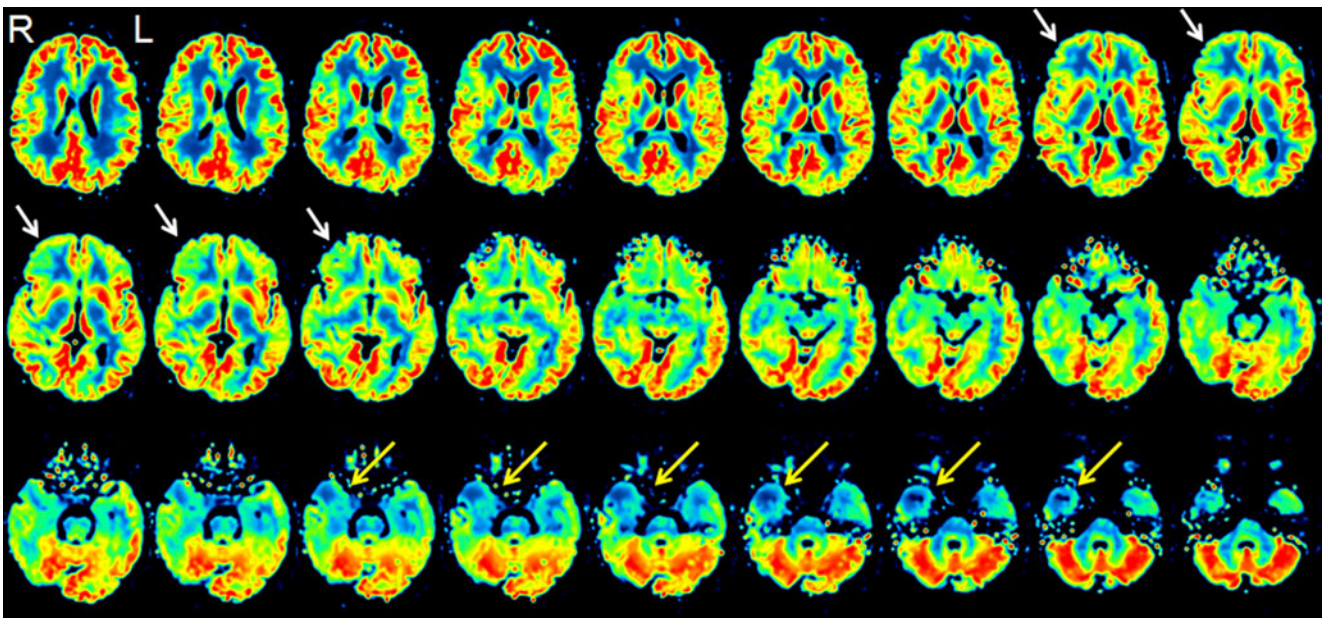

Fig. 4 A-MAP reconstructed FDG-PET images from a patient with FCD in the right temporal cortex (patient 6) show clear hypometabolism (*yellow arrows*). Visual interpretation also shows a hypometabolic area in the right inferofrontal cortex (*white arrows*), representing the functional deficit zone

reconstruction, respectively, which is in the same range as reported in the literature. A detection rate of 67% was found in extratemporal epilepsy in a meta-analysis by Casse et al. [32], and in a recent study by Salamon et al., lesions were correctly identified in 71% of patients with cortical dysplasia using blinded review of FDG-PET scans [33]. They also found a less-pronounced hypometabolism in type I FCD than in type II FCD. In individual patients, the FDG metabolism associated with the FCD was 10–75% less than that in the contralateral cerebral cortex.

We detected fewer hypometabolic cortical areas outside the FCD location using A-MAP reconstruction. This difference was on the one hand caused by a reduction in hypometabolic cortical areas in the midfrontal and posterior and superior parietal cortex regions, which was detected on ML reconstructed images but not on A-MAP reconstructed images. An example is presented in Fig. 3. These hypometabolic areas on ML reconstructed images were most likely the result of PVE, and were thus false-positive. On the other hand, hypometabolic cortical areas in the immediate surroundings of lesions detected on ML reconstructed FDG-PET images were often not visualized on A-MAP reconstructed images. Together with a higher asymmetry index of the lesion compared to normal cortex, this better delineation made it easier to detect the lesion visually on A-MAP reconstructed images. In extratemporal epilepsy, as in temporal lobe epilepsy, the hypometabolic area on FDG-PET images is often more extensive than the pathological abnormality [32]. We also found hypometabolism on ML reconstructed images and on A-MAP reconstructed images in brain regions outside the lesion, consistent with the observation that the functional deficit zone tends to be larger than the epileptogenic zone. An example is presented in Fig. 4. We speculate that this hypometabolism can be attributed to surrounding inhibition in the areas of seizure propagation, which acts as a dynamic defence mechanism against seizure propagation, and may be responsible for the deficits in executive function that are often observed in patients with temporal lobe epilepsy [21, 34].

FDG-PET/MRI coregistration has been shown to be useful in detecting cortical dysplasia in patients with epilepsy. The addition of FDG-PET/MRI coregistration to the presurgical protocol enhances the ability to detect FCD, especially in patients with type I or type II FCD and nonconcordant EEG and MRI findings. Using this approach, true-positive FDG-PET/MRI coregistration results have been found in 44/45 patients (98%) [33]. We also found an increase in the detection of hypometabolism at the location of the lesion on FDG-PET images when using FDG-PET/MRI coregistration. Our findings and those of Salomon et al. stress the importance of using coregistered FDG-PET and MR images in the presurgical protocol to improve detection of the epileptogenic lesion.

In this study, we compared A-MAP reconstruction to optimized ML reconstruction with resolution recovery. This may explain the modest improvements that we found in the detection of hypometabolic areas on FDG-PET images in our patient group. The benefit of using of the A-MAP reconstruction algorithm may therefore be greater when compared to classic ML reconstruction of brain FDG-PET data without resolution recovery or filtered back-projection, which are often used in clinical practice.

Conclusion

The A-MAP reconstruction algorithm improves the visual detection of hypometabolic epileptic FCDs on brain FDG-PET images compared to ML reconstruction, due to higher contrast and better delineation of the lesion. Hypometabolism outside the lesion is present in a majority of patients, consistent with the observation that the functional deficit zone tends to be larger than the epileptogenic zone. FDG-PET/MRI coregistration is important for optimal detection of the epileptogenic zone on both imaging modalities.

Acknowledgments K.G. is supported by a research mandate of the Flemish Fund for Scientific Research. K.V.L. is Senior Clinical Investigator of the Flemish Fund for Scientific Research. This work was partly funded by the Institute for the Promotion of Innovation by Science and Technology in Flanders (IWT-SBO), by an IAP-NIMI grant from the Belgian Science Policy and by the Interdisciplinary Research Program of the Research Fund of the K.U.Leuven (IDO3/010; fellowship F/03/027 for A.P.).

References

1. Westbrook GL. Seizures and epilepsy. In: Kandel ER, Schwarts JH, Jessell TM, editors. Principles of neural science. New York: McGraw-Hill; 2000. p. 910–35.
2. Barkovich AJ, Kuzniecky RI, Jackson GD, Guerrini R, Dobyns WB. Classification system for malformations of cortical development: update 2001. Neurology 2001;57:2168–78.
3. Sisodiya SM. Surgery for malformations of cortical development causing epilepsy. Brain 2000;123:1075–91.
4. Frater JL, Prayson RA, Morris III HH, Bingaman WE. Surgical pathologic findings of extratemporal-based intractable epilepsy: a study of 133 consecutive resections. Arch Pathol Lab Med 2000;124:545–9.
5. Palmini A, Najm I, Avanzini G, Babb T, Guerrini R, Foldvary-Schaefer N, et al. Terminology and classification of the cortical dysplasias. Neurology 2004;62:S2–8.
6. Kim DW, Lee SK, Chu K, Park KI, Lee SY, Lee CH, et al. Predictors of surgical outcome and pathologic considerations in focal cortical dysplasia. Neurology 2009;72:211–6.
7. Chugani HT, Shields WD, Shewmon DA, Olson DM, Phelps ME, Peacock WJ. Infantile spasms: I. PET identifies focal cortical dysgenesis in cryptogenic cases for surgical treatment. Ann Neurol 1990;27:406–13.
8. Chugani HT. The use of positron emission tomography in the clinical assessment of epilepsy. Semin Nucl Med 1992;22:247–53.

9. Shields WD, Shewmon DA, Chugani HT, Peacock WJ. Treatment of infantile spasms: medical or surgical? Epilepsia 1992;33:S26–31.
10. Chugani HT, Shewmon DA, Shields WD, Sankar R, Comair Y, Vinters HV, et al. Surgery for intractable infantile spasms: neuroimaging perspectives. Epilepsia 1993;34:764–71.
11. Chugani HT, Conti JR. Etiologic classification of infantile spasms in 140 cases: role of positron emission tomography. J Child Neurol 1996;11:44–8.
12. Kim SK, Na DG, Byun HS, Kim SE, Suh YL, Choi JY, et al. Focal cortical dysplasia: comparison of MRI and FDG-PET. J Comput Assist Tomogr 2000;24:296–302.
13. Otsuki T. Neuroimaging and presurgical evaluation of symptomatic epilepsies. Psychiatry Clin Neurosci 2004;58:S13–5.
14. Yun CH, Lee SK, Lee SY, Kim KK, Jeong SW, Chung CK. Prognostic factors in neocortical epilepsy surgery: multivariate analysis. Epilepsia 2006;47:574–9.
15. Fazio F, Perani D. Importance of partial-volume correction in brain PET studies. J Nucl Med 2000;41:1849–50.
16. Fischl B, Dale AM. Measuring the thickness of the human cerebral cortex from magnetic resonance images. Proc Natl Acad Sci U S A 2000;97:11050–5.
17. Baete K, Nuyts J, Van Paesschen W, Suetens P, Dupont P. Anatomical-based FDG-PET reconstruction for the detection of hypo-metabolic regions in epilepsy. IEEE Trans Med Imaging 2004;23:510–9.
18. Baete K, Nuyts J, Van Laere K, Van Paesschen W, Ceyssens S, De Ceuninck L, et al. Evaluation of anatomy based reconstruction for partial volume correction in brain FDG-PET. Neuroimage 2004;23:305–17.
19. Nuyts J, Baete K, Beque D, Dupont P. Comparison between MAP and postprocessed ML for image reconstruction in emission tomography when anatomical knowledge is available. IEEE Trans Med Imaging 2005;24:667–75.
20. Engel J Jr. Clinical neurophysiology, neuroimaging, and the surgical treatment of epilepsy. Curr Opin Neurol Neurosurg 1993;6:240–9.
21. Nelissen N, Van Paesschen W, Baete K, Van Laere K, Palmini A, Van Billoen H, et al. Correlations of interictal FDG-PET metabolism and ictal SPECT perfusion changes in human temporal lobe epilepsy with hippocampal sclerosis. Neuroimage 2006;32:684–95.
22. Talairach J, Tournoux P. Co-planar stereotactic atlas of the human brain. Stuttgart: Thieme Medical Publishers; 1988.
23. Van Laere K, Goffin K, Casteels C, Dupont P, Mortelmans L, de Hoon J, et al. Gender-dependent increases with healthy aging of the human cerebral cannabinoid-type 1 receptor binding using [(18)F]MK-9470 PET. Neuroimage 2008;39:1533–41.
24. Muller-Gartner HW, Links JM, Prince JL, Bryan RN, McVeigh E, Leal JP, et al. Measurement of radiotracer concentration in brain gray matter using positron emission tomography: MRI-based correction for partial volume effects. J Cereb Blood Flow Metab 1992;12:571–83.
25. Aston JA, Cunningham VJ, Asselin MC, Hammers A, Evans AC, Gunn RN. Positron emission tomography partial volume correction: estimation and algorithms. J Cereb Blood Flow Metab 2002;22:1019–34.
26. Zaidi H, Montandon M-L. The new challenges of brain PET imaging technology. Curr Med Imaging Rev 2006;2:3–13.
27. Knowlton RC, Laxer KD, Klein G, Sawrie S, Ende G, Hawkins RA, et al. In vivo hippocampal glucose metabolism in mesial temporal lobe epilepsy. Neurology 2001;57:1184–90.
28. Giovacchini G, Bonwetsch R, Herscovitch P, Carson RE, Theodore WH. Cerebral blood flow in temporal lobe epilepsy: a partial volume correction study. Eur J Nucl Med Mol Imaging 2007;34:2066–72.
29. Giovacchini G, Toczek MT, Bonwetsch R, Bagic A, Lang L, Fraser C, et al. 5-HT 1A receptors are reduced in temporal lobe epilepsy after partial-volume correction. J Nucl Med 2005;46:1128–35.
30. Koepp MJ, Labbe C, Richardson MP, Brooks DJ, Van PW, Cunningham VJ, et al. Regional hippocampal [11C]flumazenil PET in temporal lobe epilepsy with unilateral and bilateral hippocampal sclerosis. Brain 1997;120(Pt 10):1865–76.
31. Koepp MJ, Richardson MP, Labbe C, Brooks DJ, Cunningham VJ, Ashburner J, et al. 11C-flumazenil PET, volumetric MRI, and quantitative pathology in mesial temporal lobe epilepsy. Neurology 1997;49:764–73.
32. Casse R, Rowe CC, Newton M, Berlangieri SU, Scott AM. Positron emission tomography and epilepsy. Mol Imaging Biol 2002;4:338–51.
33. Salamon N, Kung J, Shaw SJ, Koo J, Koh S, Wu JY, et al. FDG-PET/MRI coregistration improves detection of cortical dysplasia in patients with epilepsy. Neurology 2008;71:1594–601.
34. Goffin K, Dedeurwaerdere S, Van Laere K, Van Paesschen W. Neuronuclear assessment of patients with epilepsy. Semin Nucl Med 2008;38:227–39.